Stereochemistry of post-transition metal oxides: revision of the classical lone pair model

Aron Walsh[1*], David J. Payne[2], Russell G. Egdell[2] and Graeme W. Watson[3]

[1] *Centre for Sustainable Chemical Technologies and Department of Chemistry, University of Bath, Claverton Down, Bath BA2 7AY, United Kingdom.*

[2] *Department of Chemistry, University of Oxford, Inorganic Chemistry Laboratory, South Parks Road, Oxford OX1 3QR, United Kingdom.*

[3] *School of Chemistry and CRANN, Trinity College Dublin, Dublin 2, Ireland.*

E-mail: a.walsh@bath.ac.uk

Table of Contents Entry

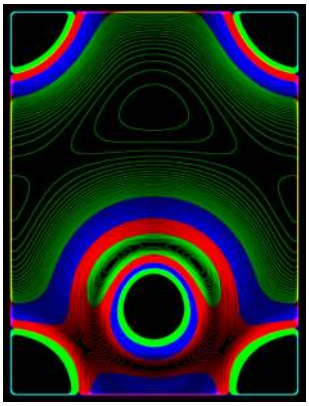

This tutorial review addresses the structural and electronic aspects of cationic lone pairs in the solid-state.

Abstract

The chemistry of post transition metals is dominated by the group oxidation state N and a lower N-2 oxidation state, which is associated with occupation of a metal s^2 lone pair, as found in compounds of Tl(I), Pb(II) and Bi(III). The preference of these cations for non-centrosymmetric coordination environments has previously been rationalised in terms of direct hybridisation of metal *s* and *p* valence orbitals, thus lowering the internal electronic energy of the N-2 ion. This explanation in terms of an on-site second-order Jahn-Teller effect remains the contemporary textbook explanation. In this Tutorial Review, we review recent progress in this area, based on quantum chemical calculations and X-ray spectroscopic measurements. This recent work has led to a revised model, which highlights the important role of covalent interaction with oxygen in mediating lone pair formation for metal oxides. The role of the anion *p* atomic orbital in chemical bonding is key to explaining why chalcogenides display a weaker preference for structural distortions in comparison to oxides and halides. The underlying chemical interactions are responsible for the unique physicochemical properties of oxides containing lone pairs and, in particular, to their application as photocatalysts ($BiVO_4$), ferroelectrics ($PbTiO_3$), multi-ferroics ($BiFeO_3$) and *p*-type semiconductors (SnO). The exploration of lone pair systems remains a viable avenue for the design of functional multi-component oxide compounds.

Keywords: Metal Oxides; Lone Pairs; X-ray Photoemission Spectroscopy; Density Functional Theory; Ferroelecticity; Photocatalysis; Semiconductors

Biographies

Aron Walsh received his BAmod (2003) and PhD (2006) in Computational Chemistry from Trinity College Dublin, Ireland. He worked as a postdoctoral researcher at the National Renewable Energy Laboratory, USA, and then at University College London as a Marie Curie Fellow. He recently joined the Department of Chemistry at the University of Bath, where his research group, in the Centre for Sustainable Chemical Technologies, focuses on the development and application of computational techniques for functional materials design and characterisation. Current interests include hybrid organic-inorganic frameworks, the defect chemistry of multi-component transparent conducting oxides, and the design of sustainable solar cell absorber materials.

David Payne received his MChem (2004) from Cardiff University and DPhil (2008), in experimental solid-state chemistry, from the University of Oxford, UK. Since 2007 he has been a Junior Research Fellow at Christ Church, University of Oxford. His interests include the spectroscopic determination of the electronic structure of oxide materials, and in particular development and characterization of new materials for solar water-splitting. Recently he has been appointed Lecturer in the Department of Materials at Imperial College London, and will take up this post in September 2011.

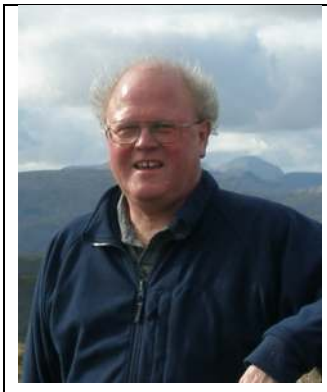	*Russ Egdell is an experimentalist working on the electronic structure and surface chemistry of metal oxides. A wide range of techniques are used in his group, including X-ray spectroscopy, electron and scanning probe microscopy, and X-ray and electron diffraction. He completed his doctorate in Inorganic Chemistry at the University of Oxford in 1977 and after 6 years as a research fellow in Oxford was appointed Lecturer in Physical Chemistry at Imperial College in 1983. He returned to Oxford in 1990 and was elevated to a Professorship in October 2000. Recent work centres on energy materials, in particular the growth of transparent conducting oxides by molecular beam epitaxy.*

	*Graeme Watson received a BSc (1990) and PhD (1994) in Computational Chemistry from Bath University, UK. Following postdoctoral research positions at Bath, Liverpool and Cardiff, he joined Trinity College Dublin as a lecturer in Computational Chemistry in 2000, followed by promotion to Senior Lecturer (2004) and Associate Professor (2006). Graeme's research involves modelling solid-state materials encompassing the electronic and optical properties, point defects, surface structure and reactivity. Areas of recent interest include oxide and metal catalysts, transparent conducting materials, photovoltaics, thermoelectrics, solid oxide fuel cells, lithium batteries and novel electronic materials.*

1. Introduction

The relationship between the atomic structure of chemical systems and their macroscopic properties is one of the most fundamental in the physical sciences. Moreover, the microscopic structure is intimately related to the local chemical bonding between the constituent elements, which may be driven by electrostatics for ionic systems (*e.g.* the octahedral rocksalt lattice of NaCl maximises the Madelung constant) or orbital hybridisation for covalent systems (*e.g.* the tetrahedral diamond lattice of Si facilitates sp^3 hybridisation).

For metal oxides hetero-polar bonds are formed between the positively charged metal and negatively charged oxygen atoms due to the large value of the electronegativity of oxygen[1]. The resulting crystal structures of metal oxides can commonly be rationalised by considering the component ions as rigid close-packed spheres with an effective ionic radius[2]. The material stoichiometry and radius ratio determine the packing, resulting in the series of high symmetry structures that are ubiquitous in inorganic chemistry. For example, for 1:1 stoichiometry the rocksalt structure with octahedral ion coordination (see Figure 1a) is favoured for cation:anion radius ratios between 0.732 and 0.414, while the zinc-blende or wurtzite structures with tetrahedral ion coordination are favoured for smaller cation:anion radius ratios. When the radius ratio exceeds 0.732, the 8 coordinate caesium chloride structure is favoured. The fundamentals of chemical stereochemistry began with the work of Lewis[3] on molecular structures, and were adapted by Pauling[4] in his rules for determining the crystal structures of polar solids. The applicability of these simple guidelines to complex multi-component compounds is well established[5]. However, exceptions emerge, especially for heavier cations, where their high electric polarizibility favours non-spherical packing of ions. Two notable cases involve d^{10} systems such as the Cu(I) ion, where hybridisation of the $3d_z^2$ and 4*s* orbitals results in the characteristic preference for linear coordination; and Hg(II) in compounds such as HgO, where the hybridisation between 5*d* and 6*s* is mediated by O 2*p*.[6] Another major exception is found for cations with a filled s^2 electron pair, which is the subject of this review.

Metals found at the lower end of groups 13-16 of the periodic table can exhibit a valence state two lower than the group valence, as in compounds of Tl(I), Pb(II), Bi(III) and Po(IV). These arise from so-called inert electron pairs. The stable $d^{10}s^2p^0$ electronic configuration results in the formal occupation of the valence metal *s* orbitals. In the theory of stereochemistry of valence bonds by Sidgwick and Powell[7], these lone pairs of electrons are on equal standing with bonded electron pairs and distribute themselves to minimise electrostatic repulsion. In the modification by Gillespie and Nyholm[8], repulsions involving one pair are recognised as being greater than those arising from standard valence bonds, which explains successfully the bond angles of ammonia and water molecules. Applied to lower valence state metals such as Pb(II), one would expect non-symmetric crystals, where the lone pair electrons occupy the corner of a polyhedron. Indeed, this is the case for PbO in the litharge structure (see Figure 1b), where all four coordinated oxygen atoms are found on one side of Pb, with the lone pair projected out in the opposite direction. What this theory does not explain is why some compounds formed from the same cation, in the same oxidation state, can exhibit stereochemically active or inactive lone pairs depending on the anion. In organometallic chemistry, these are referred to as "hemi-directed" (active) or "holo-directed" (inert) lone pairs[9].

The stability of the lower oxidation state of the metal tends to increase down a group, possibly with an alternation such that the *N*-2 state for 4th row elements is less stable than expected from a linear interpolation between 3rd and 5th rows; thus in group 14, the divalent state is increasingly favoured in going from Ge to Sn to Pb.[10] Compounds formed from the two oxidation states can exhibit very different physicochemical properties. One illuminating example is Pb, where the metallicity of black Pb(IV)O_2 is exploited in lead acid batteries[11], while Pb(II)O is an insulating red or yellow solid depending on the orientation of the lone electron pair[12].

This Topical Review provides an update of our understanding of cationic lone pair compounds, with an emphasis on solid-state systems. We highlight the structural and electronic aspects of lone pair formation in the context of recent experimental and theoretical insights into the topic. The anomaly found in the existing textbook explanation for these systems is resolved in the revised

model; the competition between centro-symmetric and distorted crystal structures is rooted fundamentally in chemical bonding that has an explicit dependence on the anion. Finally, we review recent advances in utilising lone-pair containing materials for technological applications, including photocatalysis and solar cells, and discuss avenues for future materials research based on these systems.

2. Lone Pair Formation

2.1 Classical Model

Contemporary textbooks usually refer to the classical view of the cationic lone pair as introduced by Orgel[2, 13]. In this model, the lone pair is considered to be derived from an on-site mixing of non-bonding cation *s* and *p* orbitals. Due to the fact that *s* and *p* orbitals are of different parity, mixing of this sort cannot take place on cations occupying sites with inversion symmetry. However, *sp* hybridised orbitals may be generated in non-centrosymmetric sites, thus explaining the distorted structures of many materials that have stereochemically active lone pairs. More simply, an electron repulsion treatment[8] can be used to rationalise the stereochemical consequences of the hybrid orbitals. The stabilisation of distorted structures can be considered as a second-order (or pseudo) Jahn-Teller instability: upon atomic displacement orbital (*sp*) hybridisation occurs that reduces the total energy of the system. The ground state is not degenerate in the undistorted system as in a first-order Jahn-Teller distortion, but instead the degeneracy of the lowest energy unoccupied orbital (the *p* orbital) is removed, thus allowing one component of the split *p* shell to achieve the same symmetry as the lower energy occupied *s* orbital. Mixing between these ground and excited states produces the second-order stabilisation.

However, many materials that have the required electronic configuration to form lone pairs on the cation do not display this stereochemical activity. For example, PbO and SnO adopt the litharge structure (Figure 1b), while PbS and SnTe crystallise in the perfectly symmetric rocksalt structure (Figure 1a). Orgel attempted to explain the activity of the lone pair through electric

polarisation arguments, which depend simply on the energy separation between the atomic *s* and *p* orbitals and the equilibrium bond length. Exceptions to the rule, notably for chalcogenides, are attributed to effects of covalency.

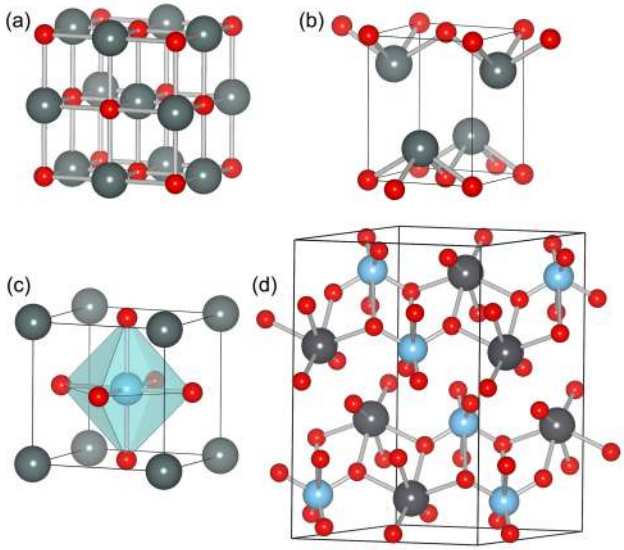

Figure 1 Crystal structure representations of the (a) rocksalt (*e.g.* MgO, SnTe), (b) litharge (*e.g.* SnO, PbO), (c) perovskite (*e.g.* $BiFeO_3$) and (d) clinobisvanite (*e.g.* $BiVO_4$) mineral structures. The cations are coloured silver, with red reserved for the anions.

Clearly the classical treatment is incomplete and does not provide an understanding of the nature of the stereochemically active lone pair and why it forms in some compounds and why it does not form in others. The diversity of crystal structures adopted by lone pair systems is highlighted in Table 1. The concept of an electron lone pair as a chemically inert species remains popular due to its ability to explain the distorted structures often observed in these materials, but it is unsatisfactory in its generality.

2.2 Revised Model

To understand the nature of lone pairs it is instructive to begin with a discussion of the interactions that occur in undistorted structures for these materials. A quantum mechanical analysis, at the level of Density Functional Theory[14, 15], of the electronic structure of PbO[16, 17] and SnO[18, 19] in the CsCl structure, the undistorted parent of the litharge structure they adopt, shows that the s^2 electrons

are certainly not chemically inert. They interact strongly with the anion *p* states in the valence band giving rise to bonding and anti-bonding states (Figure 2), which appear at the bottom and top of the upper valence band, respectively. The filled s^2 electrons of the cation do *not* form a non-bonding electron pair. So why does this interaction lead to the formation of distorted structures?

The formation of a distortion in the lattice allows the unoccupied cation *p* states to hybridize with the anti-bonding states, resulting in a stabilisation of the occupied electronic states (Figure 2). In the absence of a crystal distortion, the interaction of the cation *p* orbitals has no net stabilising effect; the interaction is composed of both positive and negative wavefunction overlap, which is forbidden by the crystal symmetry. However, by distorting the lattice, the interaction becomes symmetry allowed and the orbital stabilisation is accompanied by an asymmetric electron density that is projected into the structural void. The asymmetric electron density has the familiar lone pair distribution, but is in fact a stabilized anti-bonding interaction between the electronic states of both the cation and anion.

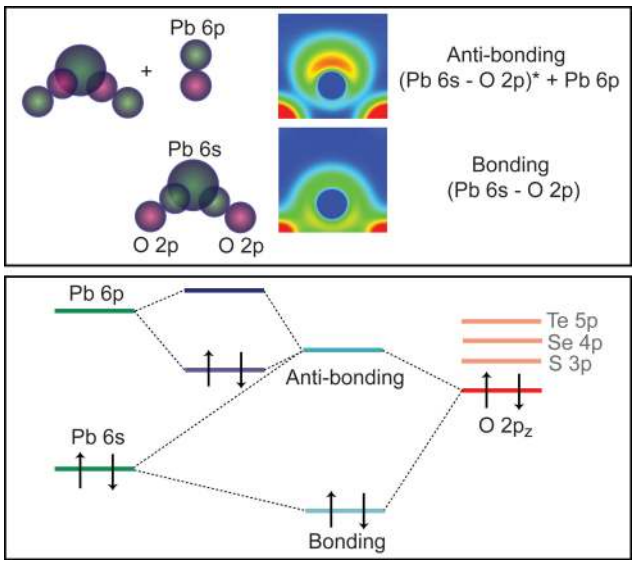

Figure 2 Illustration of the orbital interactions that lead to lone pair formation in PbO (upper panel) and the corresponding energy level diagram (lower panel).

Subsequent studies comparing PbO with PbS[20] and SnO with SnX {X=S, Se, Te}[21] have shown that computations based on quantum mechanics not only predict if a directional lone pair will form, but

also explain *why* lone pairs form in some materials and not in others. The relative energy of the cation *s* and anion *p* states is critical to the formation of stereochemically active lone pairs. Since the cation *p* states interact with the anti-bonding levels, it is vital for the cation on-site hybridisation that the anti-bonding levels have a strong component of the cation *s* states. If there is a substantial cation *s* presence, then the mixing of the cation *p* states can result in a strong stabilisation of the anti-bonding state. If, however, the anti-bonding states have only a weak contribution from the cation *s* states, then the stabilisation will be significantly weaker. The electronic stabilisation must compensate for the reduced coordination in the distorted structures, and hence materials in which the anti-bonding states have only a weak cation *s* component will not form stereochemically active lone pairs; this is the case for most metal chalcogenides as shown in Table 1b.

The formation of stereochemically active lone pairs (distorted crystal structures) is therefore dependent on the strength of the interaction between the cation *s* states and the anion *p* states, and hence on their relative energies. The closer they are in energy, the stronger the interaction and the more cation states are present in the upper valence band, leading to an active lone pair effect. In fact, the cation *s* states in these materials are lower in energy than the anion *p* states and hence the most robust (with respect to formation of undistorted structures) lone pairs are found for oxides such as PbO, SnO, Bi_2O_3, and Sb_2O_3, *i.e.* those with oxygen anions in which the *p* states are relatively low in energy. The corresponding atomic orbital energies are summarised in Figure 4b. In moving down group 16 from oxygen to sulfur, selenium and tellurium, the anion *p* states become higher in energy: as calculated at the DFT level of theory[22] the orbital energies are -9.0 eV (O); -7.0 eV (S); -6.5 eV (Se); -5.9 eV (Te); -5.6 eV (Po). It should be noted that the largest increase is observed between O 2*p* and S 3*p*, and this is where the transition from distorted to symmetric structures generally occurs. The interaction of the anion *p* states with the cation *s* states is reduced significantly for heavier anions, leading to weaker on-site hybridisation of the cation *s* and *p* states and weaker lone pairs. For the case of PbS, the sulfur anion 3*p* states are already too high in energy to maintain the stereochemically active lone pair due to the extremely low energy of the Pb 6*s* states arising from

relativistic effects, while for Sn the 5*s* states are higher in energy and the lone pair is maintained for SnS and SnSe. Tellurium has too weak an interaction with Sn 5*s* to form a lone pair distortion in its ground-state structure.

Waghmare *et al.*[23] explored the effect of anion *p* – cation *s* overlap in the distortion of the rocksalt structured chalcogenides of Ge, Sn and Pb, which follow the same trends discussed above. Similar arguments can also be made for the case of bismuth, with Bi_2O_3 and Bi_2S_3 showing stereochemically active lone pairs[24], while Bi_2Se_3 and Bi_2Te_3 do not, and for antimony, with Sb_2X_3 {X=O, S, Se} displaying stereochemically active lone pairs and Sb_2Te_3 not. In fact for the layered crystal structure adopted by Sb_2Te_3, Bi_2Se_3 and Bi_2Te_3, the anionic lone pair becomes dominant[25].

The revised lone pair (RLP) model can be summarised as follows:

- Strong interaction between the cation *s* and anion *p* orbitals results in high-energy anti-bonding states with a considerable degree of cation *s* character at the top of the upper valence band.
- Distortion of the crystal structure to allow for the interaction of the nominally empty cation *p* states with the anti-bonding orbitals results in the familiar lone pair asymmetric electron density; these are projected anti-bonding states.

3. Quantifying Lone Pair Interactions

3.1 X-ray Emission Spectroscopy (XES)

A simple and direct experimental approach to establishing the extent of orbital hybridisation between the O 2*p* states and metal n*s* states in oxides has been established by Payne *et al.*[26, 27]. It is based on comparison between Al Kα X-ray photoemission (XPS) spectra and O K shell X-ray emission spectra (XES). XPS measures the total density of states of oxides, although the contributions from the various atomic partial densities of states that are involved in the valence band must be weighted by the ionisation cross-sections for the orbitals involved. O K shell X-ray emission involves radiative decay of electrons into an O 1*s* core hole and is governed by a strict on-site dipole selection rule, which dictates that only electrons with O 2*p* character can be involved in the transition. The intensity

of a band in XES is therefore directly proportional to its O 2*p* character, and in the absence of mixing with O 2*p* states transitions from metal n*s* valence states would be completely absent. Experimental data for Bi_2O_3 are shown in Figure 3 along with the electronic density of states calculated from Density Functional Theory.

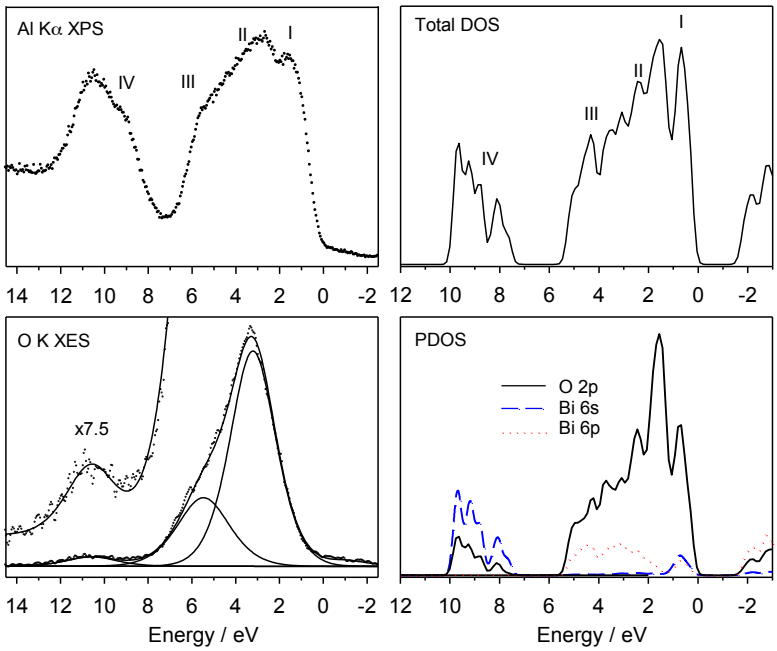

Figure 3 Valence band Al Kα XPS and O K shell XES spectra from Bi_2O_3 compared with the total and atom-projected density of states derived from quantum mechanical calculations [Adapted from Reference [27]]. The spectra are all presented on a binding energy scale referenced to the top of the valence band. XPS and XES spectra are aligned relative to each other using peak IV.

Four features labelled I-IV are observed in the XPS data for Bi_2O_3, in good agreement with the theoretical prediction. The relative intensity of these bands is very different in XES, with band IV at the highest binding energy being much weaker than in XPS. This establishes that band IV is associated with states of dominant Bi 6*s* character, weakly hybridised with O 2*p* states. There is excellent agreement with the calculated distribution of the Bi 6*s* orbital; hence, these results provide direct experimental evidence of the RLP model proposed in Section 2.2.

To quantify this idea, it is possible to make an empirical estimate of the fractional contribution f_{O2p} of O 2*p* states to the metal n*s* band. If all the states in the valence band were of pure O 2*p* character the intensity of the *s* band (I_s) relative to the total intensity of the valence band (I_{total}) would be simply *M/P* where *M* is the number of metal atoms and *P* is the total number of valence electrons pairs per formula unit (*M*=1, *P*=4 for PbO). It follows that:

$$f_{o2p} = \frac{I_s/I_{total}}{M/P}$$

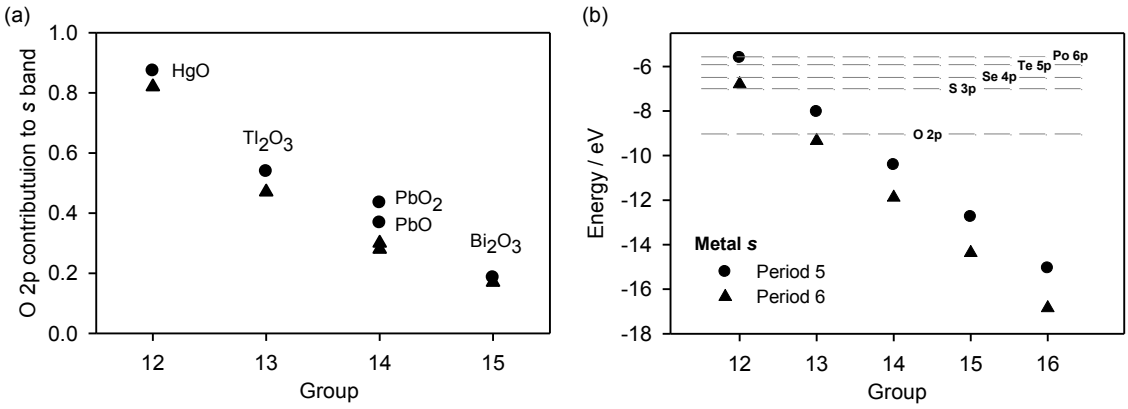

Figure 4 (a) Closed circles: estimated O 2*p* contribution to the lowest valence band state derived from intensities in the XES spectra of the post-transition metal oxides HgO, Tl_2O_3, PbO_2, PbO and Bi_2O_3 as a function of group number. Triangles: the ratio I(O 2*p*) /{I(O 2*p*)+I(M 6*s*)} derived by integrating partial densities from quantum mechanical calculations across the lowest valence band state. (b) Metal *s* and anion *p* atomic orbital energies (Kohn-Sham eigenvalues) calculated from Density Functional Theory.

For Bi_2O_3 it transpires that $f_{O2p} \approx 0.2$ so that the 6*s* "inert pair" is only weakly hybridised with the O 2*p* states[24]. Figure 4b shows results from an analysis of experimental and theoretical spectra of the oxides of Hg, Tl, Pb and Bi, including both compounds in the group oxidation state (for Hg, Tl and Pb) and the *N*-2 oxidation state (Pb, Bi). It can be seen that the extent of hybridisation between the 6*s* electrons and O 2*p* electrons decreases progressively with increasing group number as the 6*s* electrons are increasingly stabilised. The atomic energy levels of the 6*s* states increase by over 10 eV

from Hg to Po[22]: -6.8 eV (Hg); -9.3 eV (Tl); -11.9 eV (Pb); -14.4 eV (Bi); -16.8 eV (Po). It is interesting therefore to recall that PoO_2 adopts an undistorted fluorite structure, which is because the 6*s* electrons are now too far below the valence band maximum to allow for significant hybridisation with O 2*p* states. By contrast we have also seen that TeO_2 adopts structures showing the signatures of stereochemically active lone pairs: this reflects the fact that the 5*s* electrons are less tightly bound than 6s electrons because the relativistic stabilisation is much lower.

The atomic orbital trends, summarised in Figure 4b, can be used to explain the presence and strength of stereochemically active lone pair compounds: for oxides the strongest cation *s* – anion *p* hybridisation is clearly expected between Sn and O where ΔE_{s-p} = 1.4 eV (SnO forms the distorted litharge structure), whilst the weakest interaction is between Po and O as ΔE_{s-p} = 7.8 eV (PoO_2 forms the centro-symmetric fluorite structure). The resulting order of stability for lone pair distortions, Sn > Pb > Sb > Bi > Te > Po, follows the crystal structure preferences for these materials (Table 1).

3.2 Hard X-ray Photoelectron Spectroscopy (HAXPES)

While XES and XPS can reveal successfully the extent of *s* – *p* hybridisation, they are not sensitive enough to the metal *s* states to be able to observe their contributions to the valence band directly. An approach to overcome this limitation was first exploited by Payne *et al.*[28] Hard X-ray photoelectron spectroscopy (HAXPES) is a technique that is rapidly becoming the photoemission experiment of choice for researchers who require "bulk sensitive" electronic structure with minimal surface contribution, and atomic orbital selectivity. Conventional XPS (hv = 1486.6 eV (Al Kα)) has an effective probing depth of 1 – 1.5 nm, whereas for HAXPES (hv = 6 – 8 keV), the effective probing depth is of the order of 15 – 20 nm. As well as the benefits stated above, the changes in photo-ionization cross-sections, upon increasing photon energy, have a profound influence on the information obtained, regarding the orbital's comprised within the valence band of the material under study.

Taking the specific example of (structurally undistorted) PbO_2, XPS and HAXPES measurements have shown that the Pb 6*s* states do not lie at the top of the valence band, as previously assumed, but lie predominantly at the bottom, nearly 10 eV lower than the Fermi energy[28]. This result is also strengthened when used in combination with the (previously described) technique of XES as summarised in Figure 5. In the simplest description, PbO_2 has a filled valence band of O 2*p* states and an empty conduction band of Pb 6*s* states. However, in contrast to common expectations, the 6*s* contribution to conduction-band states is shown to be *less* than the contribution to the valence band, which again is supported by *ab initio* calculations.

The combination of HAXPES with element specific XES and electronic structure calculations provides a uniquely powerful and general approach to the characterization of the bulk electronic structure of oxide materials and, in particular, of the distribution of metal *s* character in structurally distorted post-transition metal oxides. This approach has already been exploited by Ogo *et al.* to study the electronic structure of SnO in the context of its semiconducting behaviour[29], and has identified the contributions of Sn 5*s* to the valence band of heavily Sn-doped In_2O_3 samples (*i.e.* ITO)[30]. HAXPES will be an essential tool for the future characterisation of lone pair containing systems.

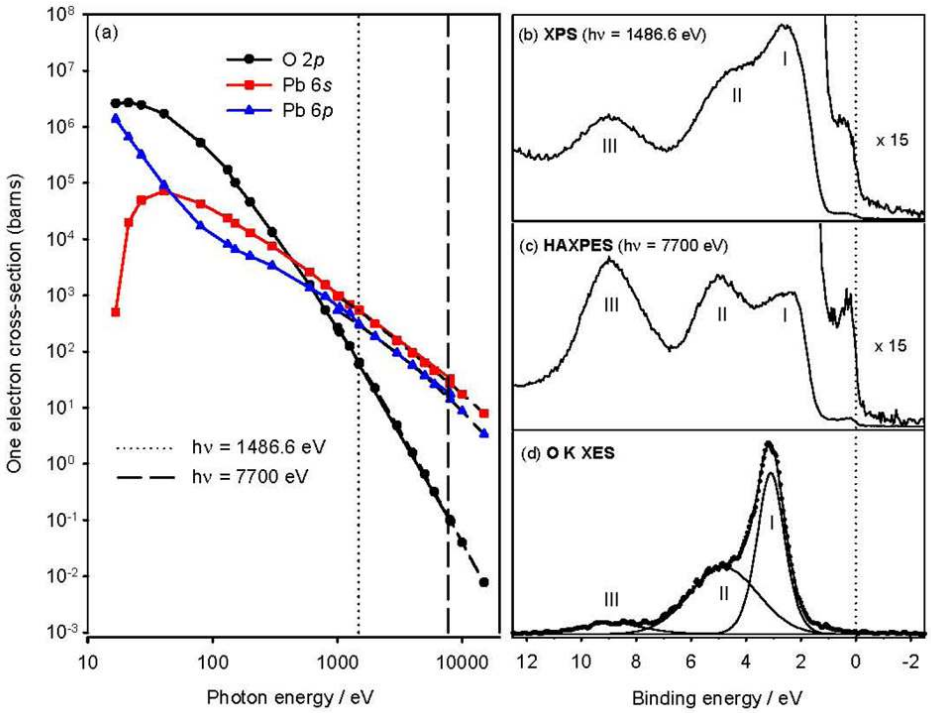

Figure 5 (a) One electron photoionisation cross-sections of Pb 6*s* (squares), Pb 6*p* (triangles) and O 2*p* (circles) orbitals as a function photon energy. Valence and conduction band photoelectron spectra of PbO_2 measured at (b) hν = 1486.6 eV and (c) hν = 7700 eV. (d) O K shell x-ray emission spectrum.

4. Property Engineering of Lone Pair Containing Oxides

4.1 Binary Oxides

Main group metal oxides are typically wide band gap materials, which have applications in catalysis, fuel cells, batteries, gas sensors, and as substrates for material growth[31]. For cations with an electronic configuration of $d^{10}s^0p^0$, such as Zn(II) and In(III), the resulting oxides are good electron conductors owing to the low carrier effective mass provided by the spatially delocalised conduction band[32]. This is also the case for the oxides of Pb(IV) and Sn(IV), as both PbO_2 and SnO_2 can support an excess of electron carriers owing to partial chemical reduction of the cations[11, 32, 33]. Indeed, Sn(II) species with active lone pairs have been characterised on the surface of SnO_2[34], where electron accumulation occurs. Occupation of the lone pair states (an electronic configuration of $d^{10}s^2p^0$) for SnO and PbO results in a substantial band structure change: both materials absorb significant

fractions of visible light, and favour *hole* over *electron* conduction. As low band gap, hole conducting oxides are a rarity, these features make lone pair systems of direct interest for electronic and optoelectronic applications, including solar energy conversion in photocatalytic and photovoltaic devices[35-37]. For further control of the material properties it is necessary to go beyond the simple binary compounds.

4.2 Ternary Oxides

Forming multi-component oxide systems introduces the possibility for property engineering through cation substitution: adjusting the crystal structure and/or composition of a material to tailor the physicochemical properties for specific applications. We will discuss a number of ternary oxides that have been of recent scientific or technological interest, before highlighting open avenues for the rational design of more complex lone pair containing solid-state systems.

4.2.1 $BiVO_4$

Bi_2O_3 is a *p*-type semiconductor, which at high temperatures converts to a fast oxygen ion conductor[38, 39]. By combining Bi_2O_3 with V_2O_5, $BiVO_4$, an active and stable photocatalyst is formed[40, 41]. Similar to Bi_2O_3 itself, the Bi coordination environment in the ternary compound is weakly distorted, forming an elongated octahedron (see Figure 1d); however, the orbital interactions involving the lone pair electrons are a key factor in determining the photoactivity of the material. It has been shown through first-principles calculations[42] and subsequent spectroscopic analysis[43] that the activity of $BiVO_4$ arises from optical transitions between anti-bonding Bi 6*s* – O 2*p* orbitals at the top of the valence band and empty V 3*d* orbitals at the bottom of the conduction band. Moreover, the filled antibonding states at the top of the valence band are key to providing the shallow acceptor levels necessary for *p*-type conductivity[44].

4.2.2 $Bi_2Sn_2O_7$

The high solubility of Bi_2O_3 with other metal oxides makes it a practical starting compound for forming more complex materials. The combination of Bi_2O_3 with SnO_2 results in the stable ternary

oxide $Bi_2Sn_2O_7$. The $A_2B_2O_7$ stoichiometry is typical of the cubic pyrochlore structure; however, to facilitate the formation of an asymmetric electron density on Bi, a $\sqrt{2}\times\sqrt{2}\times2$ monoclinic structural distortion occurs up to 130°C, resulting in a crystal structure with 352 atoms that was recently solved by X-ray diffraction[45]. For this case, the role of metal *s* – oxygen *p* hybridisation has been established[46]; however, the low phase transition temperature reflects the subtle balance between the stereochemical activity of the lone pair, and the increased coordination of the centro-symmetic phase. The calculated total energy difference between the equivalent distorted and symmetric phases reduces from 0.9 eV per formulae unit for SnO, to 0.4 eV for PbO, and just 0.2 eV for $Bi_2Sn_2O_7$ [47], which follow the trends discussed earlier.

The presence of the structural distortion for $Bi_2Sn_2O_7$ has a direct influence on the valence band position (ionisation potential)[47], which in turn will influence the catalytic properties through the stability of electronic and ionic defects on the material surface. Frustrated lone pair behaviour for another pyrochlore structured material $Bi_2Ti_2O_4$, as well as the defective pyrochlore $Pb_2Sn_2O_6$, were investigated theoretically by Seshadri[48], and this phenomenon was proposed as the source of high-*k* dielectric behaviour in this class of material system.

4.2.3 Perovskites

ABO_3 oxides adopting the cubic perovskite crystal structure (Figure 1c) are known for their ferroelectric properties: tilting and rotating the BO_2 octahedra result in electric polarisation (in response to the intrinsic dipole), and a series of ferroelectric and anti-ferroelectric phases may be accessible thermodynamically through the application of temperature, pressure and/or external lattice strain. Incorporating a lone pair cation into the lattice provides an additional driving force for non-centrosymmetric structures, as demonstrated by $PbTiO_3$, $PbVO_3$, as well as the related compounds $SnWO_4$ and $PbWO_4$[49]. The usage of lone pair cations in ternary oxides is one of the most promising routes to obtain robust multi-ferroic compounds, *i.e.* combining ferromagnetic and ferroelectric behaviour in a single material. For this purpose, one approach is to combine a lone pair "A" cation (ferroelectric component), with a magnetic "B" cation (ferromagnetic component)[50], *e.g.*

$BiFeO_3$ and $BiMnO_3$. In principle, the critical transition temperatures of these materials can be further controlled through the formation of solid-solutions or dilute doping.

4.3 Avenues for Material Design

In the last decade, there has been an upsurge in the research of lone pair containing systems. At a fundamental level, sub band-gap illumination of heavy metal oxides was found to result in a reversible red-shift in the optical absorption spectra[51], while there has been substantial technological interest in the area of photocatalysis, pioneered by the group of Kudo[52]. As discussed above, occupied cation *s* states serve both to raise the valence band energy through the addition of cation *s* – anion *p* coupling and induce lighter hole masses than typical oxides. The case of $BiVO_4$ has been discussed, and recent experimental work has identified a number of other promising candidate systems: Bi_2WO_6[53]; $Bi_{12}TiO_{20}$[54]; $BiTaO_4$[55]; Bi_2MoO_6[56]; $PbBiO_2Cl$[57]; $PbSb_2O_6$[58]; $SnWO_4$[59]; $SnNb_2O_6$[60]; Sn_2TiO_4[31].

One of the grand challenges associated with the hydrogen economy is to find a cheap and sustainable photocatalyst that would enable the generation of hydrogen from water using only sunlight. The criteria imposed on such a material are not trivial, including: visible light absorption; stability in aqueous solutions; valence and conduction bands aligned to the water redox potentials. One promising route is to combine lone pair s^2 cations (chromophores) with d^0 cations (catalytically active metals), *e.g.* $(Sn,Sb,Pb,Bi)_x(Ti,V,Nb,Mo,Ta,W)_yO_z$. Other elements can be incorporated to further tailor the properties, *e.g.* Al or Ga could increase the chemical stability or tune the band edge positions, while d^n transition metals could promote absorption of longer wavelength photons. Going beyond known or previously synthesised compounds, many mineral structures that can in principle combine these cations exist, *e.g.* the ilmenite (ABO_3), rosiaite (AB_2O_6) and trirutile (AB_2O_6) structures. There are many opportunities for material design and discovery in this area and more complex configurations that remain to be investigated.

5. Conclusions

The lone electron pair, associated with compounds formed from metals with an s^2 electronic configuration has been shown to have a strong dependence on the electronic states of the anion. The relative energy differences between the electronic states involved in the orbital interactions can explain in a straightforward manner the structural diversity of these compounds, including the strength or absence of the structural distortions associated with the lone pair of electrons. For metal oxides, the energy separation between the cation *s* and O 2*p* level follows the stereochemical activity of the lone pair: Sn > Pb > Sb > Bi > Te > Po. Experimental evidence for the role of the "inert" lone pair in chemical bonding can be achieved through the combination of electronic spectroscopies, in particular, through the application of hard X-ray photoelectron spectroscopy, which can provide bulk sensitive measurements of the metal *s* distribution in the valence band of metal oxides. The revised model provides a mechanism to understand the current generation of lone pair materials, as well as offering predictive guidance on useful combination of cations for future design of functional material systems.

Acknowledgements

A.W. acknowledges useful discussions with Alexey A. Sokol and Su-Huai Wei. G.W.W. would like to thank Stephen C. Parker for useful discussions over many years and the HEA PRTLI project IITAC and SFI PI Project (06/IN.1/I92) for funding. Many of the quantum chemical calculations reviewed in this work would not have been possible without access to the IITAC-cluster (maintained by TCHPC, Ireland); the Franklin supercomputer (maintained by NERSC, USA); the HECToR supercomputer (supported through the Materials Chemistry Consortium, UK). DJP acknowledges the support by the UK Royal Society (Research Grant RG080399) and the awards of a Junior Research Fellowship by Christ Church, University of Oxford.

References

1. C. R. A. Catlow and A. M. Stoneham, *J. Phys.: Condens. Matter*, 1983, **16**, 4321.
2. J. D. Dunitz and L. E. Orgel, *Advances in Inorganic Chemistry and Radiochemistry*, 1960, **2**, 1.
3. G. N. Lewis, *J. Am. Chem. Soc.*, 1916, **38**, 762.

4. A. Walsh and S. M. Woodley, *Phys. Chem. Chem. Phys.*, 2010, **12**, 8446-8453.
5. A. F. Wells, *Structural Inorganic Chemistry*, 5th edn., Oxford University Press, Oxford, 1984.
6. P. A. Glans, T. Learmonth, C. McGuinness, K. E. Smith, J. H. Guo, A. Walsh, G. W. Watson and R. G. Egdell, *Chem. Phys. Lett.*, 2004, **399**, 98-101.
7. N. V. Sidgwick and H. M. Powell, *Proc. R. Soc. A*, 1940, **176**, 153-180.
8. R. J. Gillespie and R. S. Nyholm, *Quarterly Reviews, Chemical Society*, 1957, **11**, 339-380.
9. L. Shimoni-Livny, J. P. Glusker and C. W. Bock, *Inorg. Chem.*, 1998, **37**, 1853-1867.
10. F. A. Cotton, G. Wilkinson, C. A. Murillo and M. Bochmann, *Advanced Inorganic Chemistry*, Wiley, New York, 1999.
11. D. J. Payne, R. G. Egdell, W. Hao, J. S. Foord, A. Walsh and G. W. Watson, *Chem. Phys. Lett.*, 2005, **411**, 181-185.
12. The actual colour depends on the polymorph."Red lead" is associated with the tetragonal litharge structure, while "yellow lead" is associated with the orthohombic massicot structure.
13. L. E. Orgel, *J. Chem. Soc.*, 1959, **1959**, 3815-3819.
14. P. Hohenberg and W. Kohn, *Phys. Rev.*, 1964, **136**, B864.
15. W. Kohn and L. J. Sham, *Phys. Rev.*, 1965, **140**, A1133.
16. G. W. Watson, S. C. Parker and G. Kresse, *Phys. Rev. B*, 1999, **59**, 8481-8486.
17. G. W. Watson and S. C. Parker, *J. Phys. Chem. B*, 1999, **103**, 1258-1262.
18. A. Walsh and G. W. Watson, *Phys. Rev. B*, 2004, **70**, 235114.
19. G. W. Watson, *J. Chem. Phys.*, 2001, **114**, 758-763.
20. A. Walsh and G. W. Watson, *J. Solid State Chem.*, 2005, **178**, 1422-1428.
21. A. Walsh and G. W. Watson, *J. Phys. Chem. B*, 2005, **109**, 18868-18875.
22. A. Walsh, University of Dublin, Trinity College, 2006.
23. U. V. Waghmare, N. A. Spaldin, H. C. Kandpal and R. Seshadri, *Phys. Rev. B*, 2003, **67**.
24. A. Walsh, G. W. Watson, D. J. Payne, R. G. Edgell, J. H. Guo, P. A. Glans, T. Learmonth and K. E. Smith, *Phys. Rev. B*, 2006, **73**, 235104.
25. J. L. F. Da Silva, A. Walsh and H. Lee, *Phys. Rev. B*, 2008, **78**, 224111.
26. D. J. Payne, R. G. Egdell, D. S. L. Law, P. A. Glans, T. Learmonth, K. E. Smith, J. H. Guo, A. Walsh and G. W. Watson, *J. Mater. Chem.*, 2007, **17**, 267-277.
27. D. J. Payne, R. G. Egdell, A. Walsh, G. W. Watson, J. Guo, P. A. Glans, T. Learmonth and K. E. Smith, *Phys. Rev. Lett.*, 2006, **96**, 157403.
28. D. J. Payne, R. G. Egdell, G. Paolicelli, F. Offi, G. Panaccione, P. Lacovig, G. Monaco, G. Vanko, A. Walsh, G. W. Watson, J. Guo, G. Beamson, P. A. Glans, T. Learmonth and K. E. Smith, *Phys. Rev. B*, 2007, **75**, 153102.
29. Y. Ogo, H. Hiramatsu, K. Nomura, H. Yanagi, T. Kamiya, M. Kimura, M. Hirano and H. Hosono, *Phys. Status Solidi A*, 2009, **206**, 2187-2191.
30. C. Korber, V. Krishnakumar, A. Klein, G. Panaccione, P. Torelli, A. Walsh, J. L. F. Da Silva, S.-H. Wei, R. G. Egdell and D. J. Payne, *Phys. Rev. B*, 2010, **81**, 165207.
31. C. R. A. Catlow, Z. X. Guo, M. Miskufova, S. A. Shevlin, A. G. H. Smith, A. A. Sokol, A. Walsh, D. J. Wilson and S. M. Woodley, *Phil. Trans. R. Soc. A* 2010, **368**, 3379-3456.
32. P. P. Edwards, A. Porch, M. O. Jones, D. V. Morgan and R. M. Perks, *Dalton Trans.*, 2004, 2995-3002.
33. K. G. Godinho, A. Walsh and G. W. Watson, *J. Phys. Chem. C*, 2009, **113**, 439.
34. M. Batzill and U. Diebold, *Prog. Surf. Sci.*, 2005, **79**, 47-154.
35. P. Veluchamy and H. Minoura, *Appl. Phys. Lett.*, 1994, **65**, 2431-2433.
36. Y. Ogo, H. Hiramatsu, K. Nomura, H. Yanagi, T. Kamiya, M. Hirano and H. Hosono, *Appl. Phys. Lett.*, 2008, **93**, 032113.
37. A. Walsh, K.-S. Ahn, S. Shet, M. N. Huda, T. G. Deutsch, H. Wang, J. A. Turner, S.-H. Wei, Y. Yan and M. M. Al-Jassim, *Energy & Environmental Science*, 2009, **2**, 774.

38. P. D. Battle, C. R. A. Catlow, J. W. Heap and L. M. Moroney, *J. Solid State Chem.*, 1986, **63**, 8-15.
39. A. Walsh, G. W. Watson, D. J. Payne, R. G. Egdell, J. Guo, P.-A. Glans, T. Learmonth and K. E. Smith, *Phys. Rev. B*, 2006, **73**, 235104.
40. K. Sayama, A. Nomura, Z. Zou, R. Abe, Y. Abe and H. Arakawa, *Chem. Commun.*, 2003, 2908.
41. I. C. Vinke, J. Diepgrond, B. A. Boukamp, K. J. de Vries and A. J. Burggraaf, *Solid State Ionics*, 1992, **57**, 83.
42. A. Walsh, Y. Yan, M. N. Huda, M. M. Al-Jassim and S.-H. Wei, *Chem. Mater.*, 2009, **21**, 547.
43. D. J. Payne, M. Robinson, R. G. Egdell, A. Walsh, J. McNulty, K. E. Smith and L. F. J. Piper, *Appl. Phys. Lett.*, 2011, **In Press**.
44. W.-J. Yin, S.-H. Wei, M. M. Al-Jassim, J. Turner and Y. Yan, *Phys. Rev. B*, 2011, **83**, 155102.
45. I. R. Evans, J. A. K. Howard and J. S. O. Evans, *J. Mater. Chem.*, 2003, **13**, 2098-2103.
46. A. Walsh, G. W. Watson, D. J. Payne, G. Atkinson and R. G. Egdell, *J. Mater. Chem.*, 2006, **16**, 3452-3458.
47. A. Walsh and G. W. Watson, *Chem. Mater.*, 2007, **19**, 5158.
48. R. Seshadri, *Solid State Sci.*, 2007, **8**, 259-266.
49. M. W. Stoltzfus, P. M. Woodward, R. Seshadri, J. H. Klepeis and B. Bursten, *Inorg. Chem.*, 2007, **46**, 3839.
50. R. Ramesh and N. A. Spaldin, *Nature Materials*, 2007, **6**, 21-29.
51. J. Heo and C. Quan, *J. Am. Ceram. Soc.*, 2010, **93**, 913-914.
52. A. Kudo and Y. Miseki, *Chem. Soc. Rev.*, 2009, **38**, 253.
53. H. Fu, C. Pan, W. Yao and Y. Zhu, *J. Phys. Chem. B*, 2005, **109**, 22432.
54. J. Hou, Y. Qu, D. Krsmanovic, C. Ducati, D. Eder and R. V. Kumar, *Chem. Commun.*, 2009, 3937.
55. R. Shi, J. Lin, Y. Wang, J. Xu and Y. Zhu, *J. Phys. Chem. C*, 2010, **114**, 6472-6477.
56. Y. Shimodaira, H. Kato, H. Kobayashi and A. Kudo, *J. Phys. Chem. B*, 2006, **110**, 17790-17797.
57. Z. Shan, X. Lin, M. Liu, H. Ding and F. Huang, *Solid State Sci.*, 2009, **11**, 1163-1169.
58. H. Mizoguchi and P. M. Woodward, *Chem. Mater.*, 2004, **16**, 5233.
59. I.-S. Cho, C. H. Kwak, D. W. Kim, S. Lee and K. S. Hong, *J. Phys. Chem. C*, 2009, **113**, 10647-10653.
60. Y. Hosogi, Y. Shimodaira, H. Kato, H. Kobayashi and A. Kudo, *Chem. Mater.*, 2008, **20**, 1299.

Table 1 The crystal structures of heavy metal oxides and chalcogenides, where *P* represent the period of the periodic table for groups 14, 15 and 16.

(a) Oxides

	14	**15**	**16**
***P*=5**	**SnO** Litharge - 4 coordinate PbO structure.	**Sb_2O_3** Orthorhombic valentinite – infinite double chains with O-Sb-O bond angles of 81°, 93° and 99°. Cubic senarmontite – molecular Sb_4O_6 units.	**TeO_2** Tellurite – layer structure with O atoms at 4 corners of trigonal bipyramid with one equatorial position vacant. Pairs of TeO_4 units share O-O edges of equatorial atoms. Paratellurite – 3D structure with local Te corrdination similar to tellurite.
***P*=6**	**PbO** Litharge.	**Bi_2O_3** α – monoclinic. β – tetragonal. γ – cubic: defective fluorite.	**PoO_2** Fluorite.

(b) Chalcogenides

	14	**15**	**16**
***P*=5**	**SnS / SnSe** Black P structure with 3 chalcogenide next nearest neighbour and local C_{3V} symmetry. **SnTe** Rocksalt.	**Sb_2S_3 / Sb_2Se_3 / Sb_2Te_3** Sulfide and selenide – the stibnite structure with sheets of Sb_2S_3 stacked along the orthorhombic *c* axis. Telluride – a rhombohedral layer structure with Te lone pairs.	**TeS_2 / $TeSe_2$** Unknown.
***P*=6**	**PbS / PbSe / PbTe** Rocksalt.	**Bi_2S_3 / Bi_2Se_3 / Bi_2Te_3** Sulfide – stibnite. Selendide and telluride – a rhombohedral layer structure with Se/Te lone pairs.	**PoS_2 / $PoSe_2$ / $PoTe_2$** Unknown.